Self-directed Transport on Nanostructured Plasmonic Sensors

Shailabh Kumar

Abstract Analytical sensors using varying detection strategies have been widely and successfully employed for advances in areas such as drug discovery, disease diagnosis and study of biological systems. Many of these sensors utilize plasmonic metallic nanostructures which can concentrate electromagnetic fields in nanoscale regions leading to many fold enhancement in optical signal obtained from the molecules. They employ techniques including fluorescence, surface plasmon resonance (SPR)-based refractive index sensing, surface-enhanced Raman spectroscopy (SERS) and other forms of vibrational spectroscopy for molecular characterization. However, the performance of these devices relies on effective transport of the target molecules to these nanoscale detection sites. Guided transport is extremely important for fast detection in cases where the concentration of molecules is really low and for accurate measurements of protein–protein binding kinetics. In this chapter, we discuss nanostructured biosensing substrates which can spontaneously direct the flow of molecules in solution towards the sensing hotspots. These devices demonstrate improved detection sensitivity, while minimizing the limitations and complexity imposed upon the system. Additionally, they can trap biological particles such as organelles and liposomes on the sensor surface, facilitating on-chip analysis of single particles. This chapter discusses a few methods which have been utilized for concentration of molecules on plasmonic sensing surfaces, without the application of external power sources.

1 Plasmonic Sensors and the Diffusion Limit

Plasmonic sensors rely on concentration of electromagnetic fields near their surface resulting in largely amplified optical signal from molecules. This signal can be collected in several forms including fluorescence, luminescence, Raman vibrational

S. Kumar (✉)
Department of Medical Engineering, California Institute of Technology, Pasadena, CA 91125, USA
e-mail: shailabh@caltech.edu

S.-H. Oh et al. (eds.), *Miniature Fluidic Devices for Rapid Biological Detection*, Integrated Analytical Systems, https://doi.org/10.1007/978-3-319-64747-0_4

spectra and SPR-based refractive index change. Since the signal is concentrated in nanoscale regions, guided transport of molecules to these sensing locations is needed. In the absence of guided transport random diffusion of molecules can result in extremely slow detection specially at low concentration levels. In a report, Sheehan and Whitman suggested that detection of molecules at sub-picomolar concentrations on nanoscale sensors would take hours to days, if left to diffusion of molecules [1]. This leads to inefficient detection of biomarkers and inaccurate mass-transport limited analysis of target-receptor interactions being studied. This critical role played by mass-transport and its interplay with receptor-target molecule binding reaction for micro- and nanoscale sensors has been extensively discussed by Squires et al. [2].

Several methods to promote the transport of molecules to the nanoscale sensing sites have been tried. Microfluidic channels with pressure-driven convective flow were utilized to maintain the supply of analytes to receptors on the sensor surface. However it was realized that convective flow over the sensors has limited benefits, due to the formation of a depletion zone near the sensing site [2, 3]. Furthermore since most of the analytes in this case flow over the substrate and do not interact with the receptors, this method is very wasteful towards expensive and difficult to extract analyte molecules. More direct means of controlling molecular transport were attempted. Pressure-driven flow was used to drive aqueous solution through plasmonic nanochannels [3–5]. Electric fields have also been employed to generate flow using electric field gradient focusing or dielectrophoresis [6–8]. However these methods suffer from key drawbacks in terms of portability and ease-of-application. Pressure-driven flow through nanochannels deals with problems derived from a high-pressure environment including leakages, damage to the nanochannels in fragile systems and fluctuation of optical signal. Similarly, electric field derived methods either rely on the charge on the molecules, or are limited by factors such as solution conductivity making it difficult to use them with biological fluids containing various molecules and ions. The requirement for external power sources also limit their portability.

Therefore, miniature fluidic devices which can generate fluidic flow spontaneously towards the sensing spots are a much desired option for diagnostic devices. In this chapter we will discuss generation of flow on nanostructured optical sensing chips using phenomena such as evaporation, surface-tension, and magnetic forces. These methods do not require any external power supplies, can be used for biological liquids such as blood and do not generate any local heating effects. Their application for efficient on-chip molecular sensing as well as trapping and analysis of biological particles will be discussed. Trapping of complex biological particles such as cells and organelles on chip can be used in combination with sensing techniques to understand cell-membrane interactions as well as their functionality.

2 Evaporation-Driven Flow

An example of evaporation-driven aggregation of particles is the famous coffee-stain effect, where the edge of the stain is much darker than the central regions. This effect can be explained by generation of localized flow towards the pinned edges of a drop of liquid on a surface [9]. The loss of water from the drop through evaporation is replenished by generation of flow from other areas towards the pinned edges, since the drop maintains its contact area on the surface. As a result, particles are transported towards this pinned edge and are concentrated there. This idea can be utilized at any pinned liquid–air interface.

Metallic nanohole arrays were chosen as the plasmonic substrate of choice for application of this technique. Metal-coated sub-wavelength nanoholes have been extensively utilized as an extremely efficient and popular plasmonic sensing devices [10–13]. They have enabled measurement of SPR-based real-time binding kinetics of molecules and proteins [14–16], SERS [14, 17, 18], and plasmon-enhanced fluorescence [19, 20]. These nanoholes have been fabricated on substrates such as glass or silicon wafers as dead-ended holes as well as in thin (hundreds of nanometers) freely hanging silicon nitride membranes which are open on both sides (open-ended nanoholes also called nanopores). Solid-state nanopores fabricated in freely hanging membranes have also been applied for DNA sequencing and single-molecule sensing. These open-ended holes have a great potential for spontaneous concentration of biomolecules.

Figure 1 shows one of the standard methods used to fabricate these holes. Photolithography and KOH wet etching were used on silicon wafers with layers of low-stress nitride to create the freely hanging nitride membranes [21]. A layer of gold was deposited on top of the membranes and focused ion beam milling was used to fabricate these structures. Nanoholes of sizes ranging from 200 to 600 nm were milled. When a drop of aqueous solution was added to these substrates, the solution was wicked into the holes due to capillary effect. In the absence of other external forces, the capillary effect does not allow the solution to flow out of the nanoholes. Hence, a water–air interface inside each of the nanohole is created, where evaporation can take place. For the solution inside the nanoholes, loss of volume due to evaporation is replenished by generation of a localized flow towards the holes, similar to pinned edges discussed earlier [9]. This results in transport of any molecules or particles in solution towards the nanoholes.

Molecules in solution can be captured by receptors present at the nanoholes and the continuous flow helps maintain the supply of the molecules to these sites. The performance of this platform was tested for protein concentration and on-chip biosensing. The chip was coated with a conformal layer of silica using atomic layer deposition (ALD). Silane-PEG-biotin was then added to the chip, forming a monolayer of biotin on the surface due to silane-silica binding. A drop of streptavidin, R-phycoerythrin conjugate (SAPE) solution was added to the chip and the effect of evaporation-driven transport was studied. As shown in Fig. 2, compared to a control region with dead-ended holes, significant concentration of the molecules

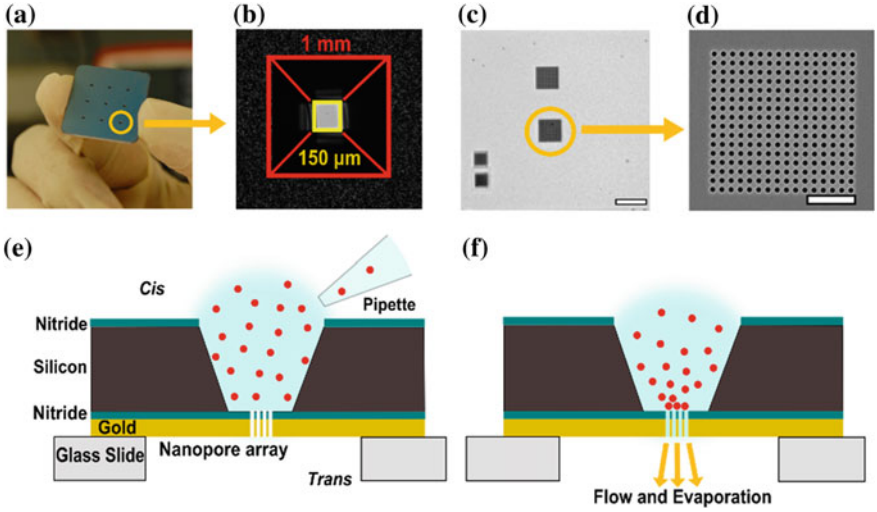

Fig. 1 **a** Chip with nine etched reservoirs. **b** Bright-field image with outlines showing a pyramidal reservoir leading to freely hanging nitride membrane. **c** Bright-field image of the membrane after milling 4 nanohole arrays. Scale bar is 20 µm. **d** Scanning electron micrograph of a nanohole array (hole diameter: 600 nm, periodicity: 1 µm) milled using focused ion beam. Scale bar is 5 µm. **e**, **f** Schematics showing the evaporation-driven mechanism of guided transport towards the holes. Reprinted with permission from [21]. Copyright 2013 American Chemical Society

can be observed at the open-ended nanoholes. This highlights the difference between diffusion-limited transport at the dead-ended holes and directed transport at the open-ended nanohole region. The results show detection of 100 pM streptavidin over the nanoholes using this method.

As mentioned earlier, gold-coated nanoholes are efficient plasmonic sensing substrates. To demonstrate the potential of label-free plasmonic sensing together with evaporation-driven concentration on these chips, SPR-based refractive index measurements were performed. These measurements are performed by recording the transmission spectra of light through the nanoholes, and monitoring the shift in peaks or dips in the spectra. The peak-shift is directly related to the local refractive index close to the nanohole hotspots. Hence binding or unbinding of molecules causes a proportional increase or decrease in the local refractive index, reflected in the peak-shift of the transmission spectra. Figure 3 shows the detection of streptavidin binding on chip at various concentrations using spectra-shift. As seen by these results, the on-chip concentration mechanism helps lower the limit of detection of the sensor by transporting molecules to nanoscale sensing locations. It works within a time-span of minutes, does not require external appendages, power sources and does not place any restrictions on the setup.

This platform and evaporation-driven transport was also utilized for capture of single organelles into the nanoholes [22]. The holes can act as reservoirs where the properties of the organelles can be analyzed individually, while they are arranged in

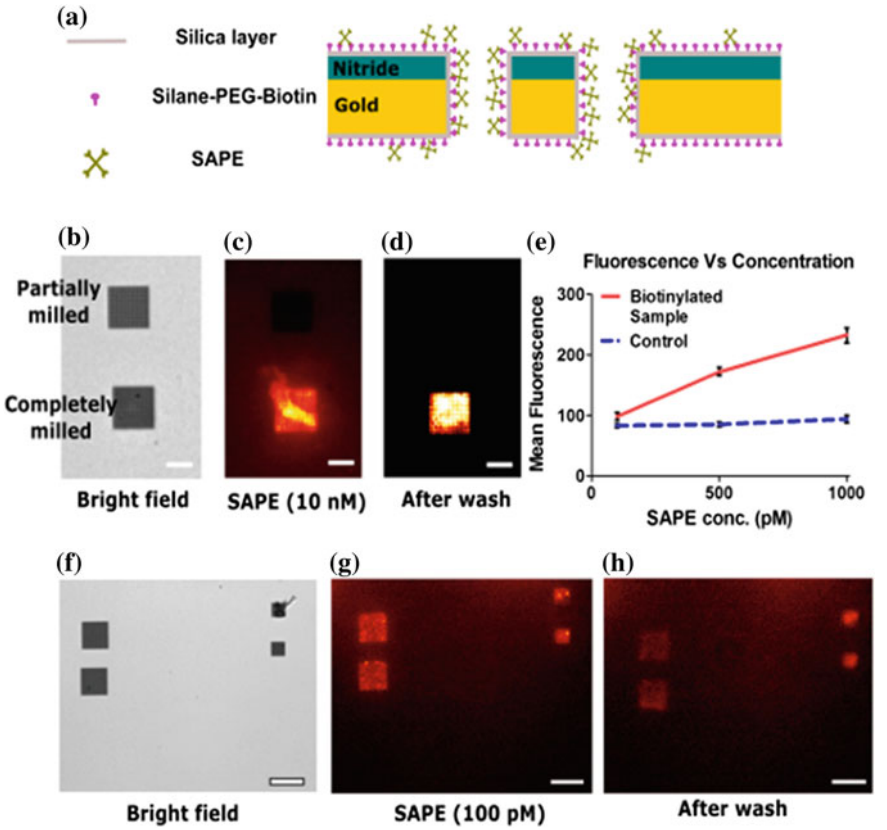

Fig. 2 **a** The chip was coated with a layer of silica followed by silane-PEG-biotin. A solution of SAPE (Streptavidin, R-Phycoerythrin conjugate), which binds to biotin, was added on to the chip. **b** A region with a partially milled nanohole array (dead-ended, control) and an array with completely milled holes (open-ended) were fabricated. **c** Fluorescence image of the sample after addition of 10 nM SAPE solution demonstrating evaporation-driven concentration. **d** Fluorescence image of the sample after rinsing the chip with DI water. **e** A graph showing the mean fluorescence over the holes as a function of SAPE concentration. **f** A suspended nitride region with 4 nanohole arrays. **g** Fluorescence image of the sample 10 mins after addition of 100 pM SAPE solution. **h** Fluorescence image after rinsing the chip with DI water. Scale bar is 10 μm for (**b**, **c**, **d**) and 20 μm for (**f, g**, **h**). Reprinted with permission from [21]. Copyright 2013 American Chemical Society

a large array. Mitochondria samples were obtained, where one batch had the membranes labeled with MitoTracker Green fluorophore and the other half expressed a fluorescent protein, DsRed2. A drop of solution with mitochondria was added to the substrate and allowed to sit for 10 mins. The sample was then washed with buffer and images were taken as shown in Fig. 4. Due to the evaporation-driven flow, organelles were transported towards the holes where they were trapped. Equal volumes of the two differently labeled mitochondria samples

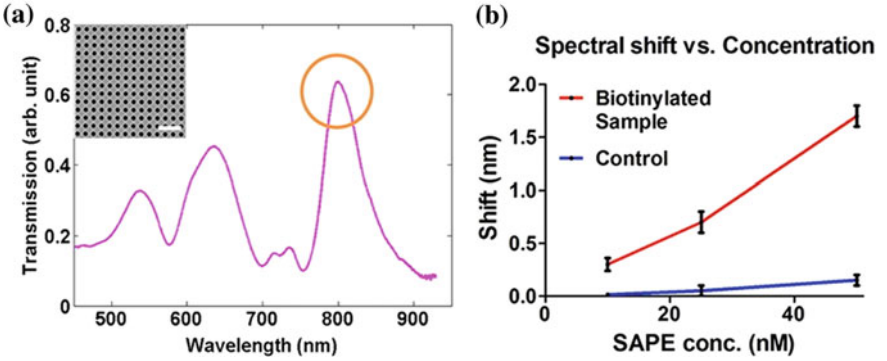

Fig. 3 Surface plasmon resonance detection of SAPE-biotin binding. **a** Normalized transmission spectra as recorded from an array of 200 nm nanopores. The transmission peak at approximately 800 nm corresponds to the gold–water interface and was used to measure the shift in transmission. (inset) SEM image of nanopores (diameter: 200 nm; periodicity: 500 nm) used for spectral measurements. Scale bar is 1.5 μm. Four arrays were milled on the suspended nitride area for measuring the transmission spectra, two large (16 μm × 16 μm) and two smaller (8 μm × 8 μm). **b** A graph showing shift of transmission spectra through the nanopore arrays upon SAPE binding as a function of SAPE concentration. Reprinted with permission from [21]. Copyright 2013 American Chemical Society

were mixed together and added to the chips. Imaging of the sample after washing indicated the presence of single color from most of the holes (Fig. 4c). The lack of color colocalization meant that individual mitochondria were trapped in single nanoholes predominantly. The membrane properties of trapped mitochondria were studied on chip using fluorescent markers of mitochondria function [22].

These results reveal the potential of an evaporation-based delivery scheme on nanoplasmonic sensors. This method increases device performance by performing analyte concentration and lowering the limit of detection. Biological particles can be trapped at nanostructured sites, without the need for any chemical modification of the surface, enabling their on-chip analysis. The platform itself is very simple to use as it does not require any assemblies, external power sources or training. Simply addition of a droplet on to the chip is sufficient to enable concentration of molecules. The limitations of this method include reliance on rate of evaporation which can be dependent on many factors such as area of the liquid–air interface and ambient conditions.

3 Surface-Tension-Based Concentration

The rate of evaporation for aqueous solutions can be slow, dependent on the fluidic volume and ambient conditions. Hence other strategies which can work with larger volumes and promote faster concentration of analytes would be advantageous.

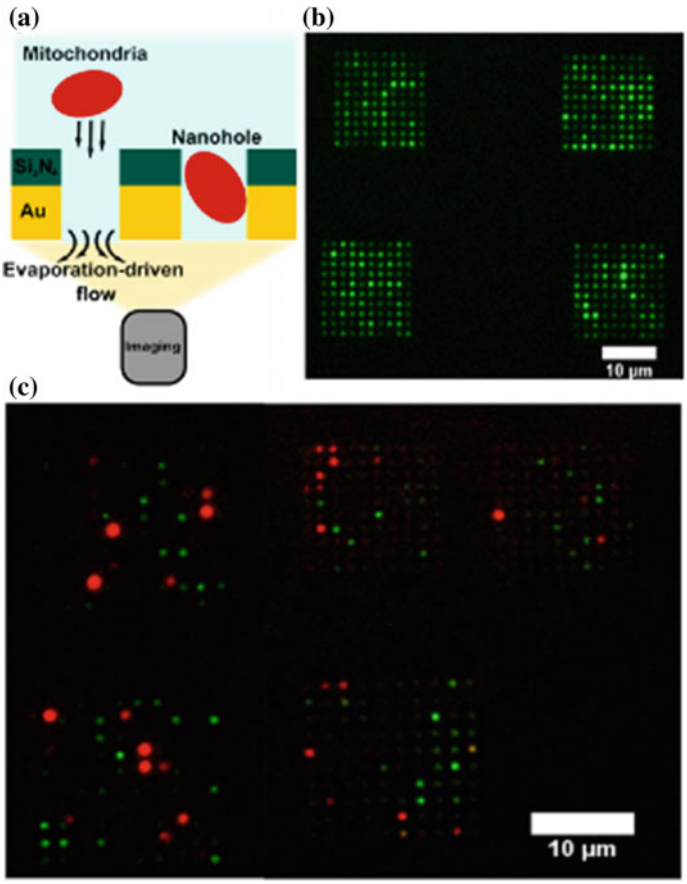

Fig. 4 **a** Mitochondria were allowed to assemble on to the nanoholes as a result of evaporation-driven transport. The samples were washed and imaged from the gold-coated end of the nanoholes. **b** Image shows 4 arrays containing trapped mitochondria tagged with MitoTracker Green dye. **c** Two samples containing mitochondria tagged with a fluorescent marker (DsRed2 in one sample and MitoTracker Green in the other) were diluted and mixed. The mixed mitochondria suspension was then added to the chip over the nanohole arrays for the capture of mitochondria. Image shows 5 arrays containing captured mitochondria tagged with either DsRed2 or MitoTracker Green. Adapted with permission from [22]. Copyright 2015 American Chemical Society

The difference in surface interaction of fluids to various surfaces can be used to drive their flow. This method takes advantage of difference in affinity of surfaces towards water. This method was employed for a microfluidic platform, demonstrating that hydrophobic patterning of microfluidic channels in combination with pressure-driven flow can control the direction of flow as well as split the flow into nanoliter-sized droplets [23]. Another application was shown by Beebe et al. using self-assembled monolayers inside microfluidic channels and creating hydrophilic

pathways in order to control fluid flow [24]. Moving towards biosensing applications, another report demonstrated an inexpensive fluidic substrate prepared with hydrophobic paper. Hydrophilic silica nanoparticles were assembled on the substrate defining the path of fluid flow. Luminol-based detection of hemoglobin was demonstrated using the paper–silica hybrid [25]. Efficient transfer of this method to nanoplasmonic sensors directing transport of molecules to the sensing hotspots would enable nanoscale flow control.

In order to transfer this idea to plasmonic substrates, nanohole arrays fabricated in freely hanging silicon nitride membranes were again utilized. Nanoimprint lithography was utilized to fabricate a 1 mm × 1 mm region of freely hanging nanohole arrays. A silicon mold with nanopillars, diameter 200 nm, height 300 nm and periodicity 500 nm was used to imprint nanohole patterns into a resist layer. The resist layer was used as a mask to transfer these patterns into the silicon nitride layer on the chips. A layer of noble metal (gold or silver) was deposited on the substrates. As shown in Fig. 5, nanoimprinting allows reproducible fabrication of nanostructures over a large region. The same mold can be used several times, thus making the process scalable, reproducible, and reducing expenses.

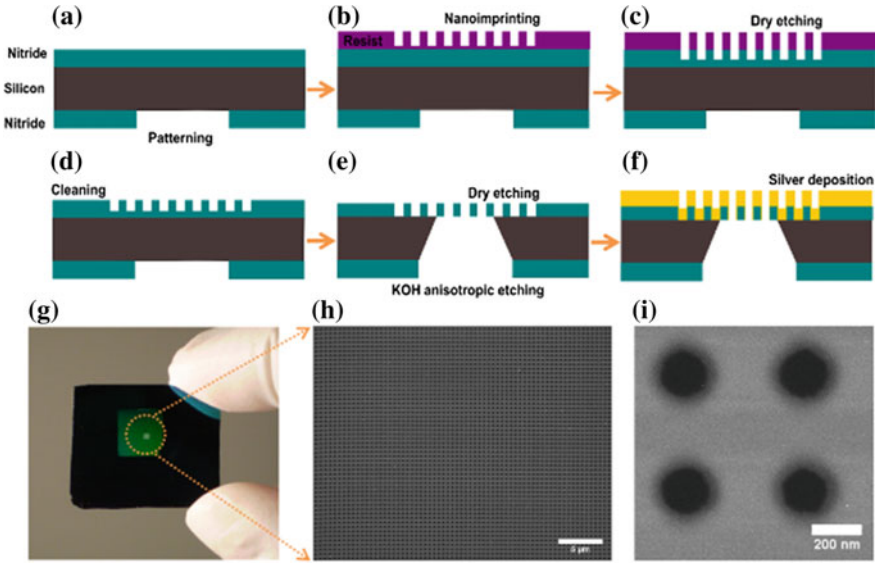

Fig. 5 **a** Deposition of 200 nm low-stress nitride and photolithography on a silicon chip. **b**, **c**, **d** Nanoimprinting, dry etching and cleaning to transfer the nanohole array pattern to the top nitride membrane. **e** Anisotropic KOH etching of silicon. A final dry-etch to remove the remaining nitride from the bottom of the holes. **f** Silver evaporated from the top to obtain freely hanging metallic nanohole arrays. **g** A 1 inch × 1 inch chip with a 1 cm × 1 cm nanoimprinted region in the center. The nanoimprinted region further has a 1 mm × 1 mm nitride membrane in the center. (Circled) **h** SEM image of a nitride membrane with nanoholes. **i** SEM shows magnified image of the individual nitride nanoholes. Adapted from [26]

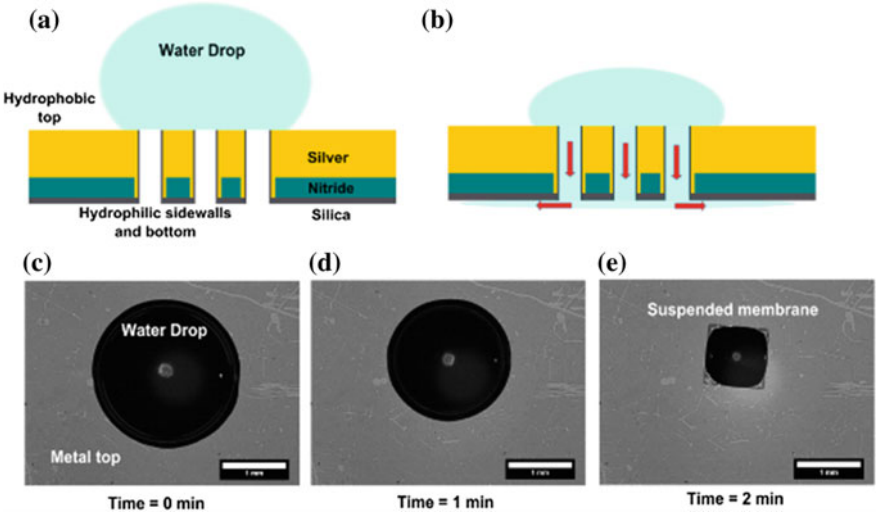

Fig. 6 **a** Addition of an aqueous droplet on the chip. The top metal surface is relatively hydrophobic as compared to the silica layer within the holes and on the backside of the chip. **b** Solution driven into the nanoholes when they come into contact with the hydrophilic sidewalls. **c**, **d**, **e** Flow of a 2 μL drop of water through the nanohole array within 2 min. The water drop shrinks as it is sucked in through the nanoholes. Adapted from [26]

The layer of metal on top of the nanostructures makes the substrate plasmonically active. A layer of silica was deposited on the backside of the chip, such that the nanohole sidewalls were also coated (Fig. 6). The noble metal layer is relatively hydrophobic compared to the silica layer. As a result, when a drop of aqueous solution was placed on the top metal surface, it was driven into the hydrophilic nanopores and flowed onto the backside of the chips. A flow rate of about 1 μL/min was generated for membranes of size 1 mm^2, which compares well to standard on-chip microfluidics. Fluid volume on the order of tens of microliters was easily transported through the holes within minutes. When compared to evaporation-driven concentration on the same chips, surface-tension-driven flow was found to be 10 times faster and the degree of concentration was about an order of magnitude higher as well [26, 27]. The plasmonic hotspots for the nanoholes are located along the edge of the nanoholes at the metal–water interface and the sidewalls. The flow of analyte molecules through the holes forces them to travel close (<100 nm) to the plasmonic hotspots. This distance is small enough to be overcome by diffusion of molecules, such that molecules can bind at or close to the plasmonic hotspots.

In order to test the sensing performance of this device, 10 μL droplets of 4-mercaptopyridine (4-MP) were added to the chips and allowed to flow through the nanoholes. SERS signal from the chips was measured using a 785 nm laser. The signal was compared with control chips which had diffusion-limited binding only. A signal enhancement of 50 times over diffusion-limited substrates was observed for these samples. A low concentration sample containing 50 pM 4-MP was

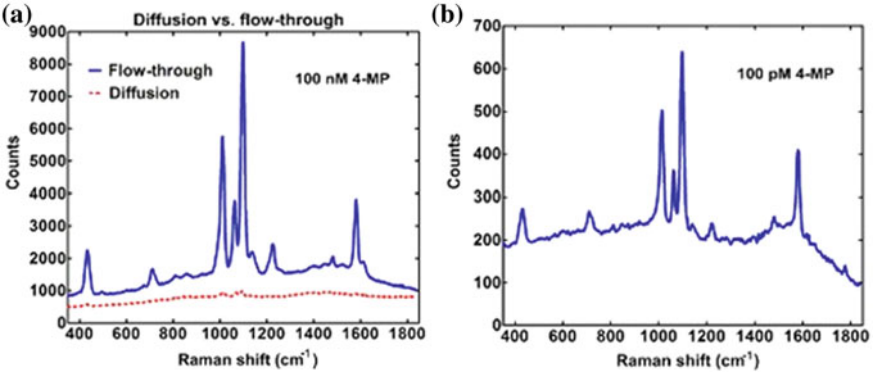

Fig. 7 **a** Comparison of SERS spectra obtained from directed transport of 100 nM 4-MP (blue spectrum) as compared to diffusion-limited transport (red). **b** SERS spectra obtained after flow of 100 pM 4-MP through the nanoholes for an hour. Adapted from [26]

detected after flow through the nanoholes for an hour, demonstrating the ability of the substrates to detect low concentration analytes. The improved sensing efficiency of these plasmonic substrates was due to the excellent plasmonic enhancement and the surface-tension directed delivery of molecules to the hotspots (Fig. 7).

As discussed, the surface-tension directed method was reported to be an order of magnitude faster and a much more efficient concentrator than the evaporation-driven method. It also has applications towards labeled or label-free sensing as well as trapping of particles at plasmonic nanostructured locations. The limitations of this method lie with the need for surface-patterning to create hydrophilic pathways. This can pose some restrictions on attachment of receptors or molecules on the fluidic pathway, which can alter the wettability of the surface.

Some other highly efficient methodologies have been used, which combine surface-patterning with evaporation-driven concentration [28, 29]. These techniques have tried to eliminate the pinning of evaporating aqueous droplets on the substrate surface, and forcing the shrinking droplets to be confined to the sensing region (Fig. 8). The evaporation of the droplet without any surface pinning forced the molecules into a smaller volume, concentrating the molecules and depositing them in an area on the order of 10 μm^2. A substrate with super-hydrophobic surface and plasmonic nanostructures was used [28], enabling molecules to be detected at attomolar concentrations.

Another example allowed molecules and plasmonic gold nanoparticles to evaporate together on a surface, while avoiding pinning of the droplet [29]. Drying droplet concentrated the molecules and gold nanoparticles in a very small region, where SERS measurement was performed. Molecules were detected at sub-femtomolar concentrations using this technique [29].

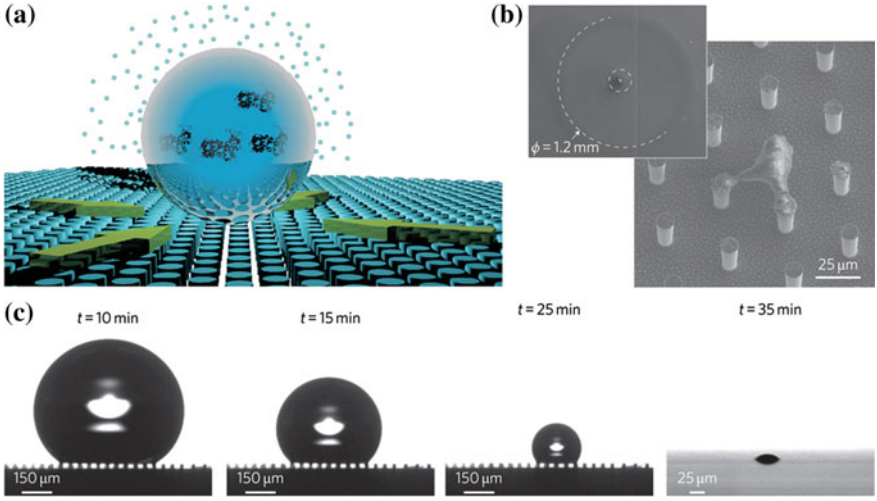

Fig. 8 **a** A schematic representing evaporation process on a super-hydrophobic surface with no pinning of the drop and no solute left on the substrate during drop concentration. **b** SEM images showing the footprint diameter of the drop and deposition of the solute on pillars. The whole content of the drop, with an initial contact area of 1.2 mm (original diameter, 2 mm), is localized on a triangle with lateral sides of ~25 μm after evaporation. **c** Images showing the evaporating droplet on the super-hydrophobic surface. The drop slips on the surface, keeping the contact angle and the shape of the drop constant. The final image shows the collapsing condition of the droplet. Reprinted by permission from Macmillan Publishers Ltd: Nature Photonics (De Angelis et al.) [28], Copyright (2011)

4 Magnetic Concentration in Fluidic Systems

Magnetic forces are well suited to work in complex biological media, including conductive and non-transparent solution like blood. Small magnets can be easily integrated with on-chip fluidic systems. They require no additional power sources, and can create extremely strong magnetic field gradients on the chip-scale. They are generally used in conjugation with magnetic particles with sizes ranging from microns to tens of nanometers. These particles offer a high surface area to volume ratio and can be chemically functionalized with different receptors for various bioassays [31]. Magnetic nanoparticles have been used for aptamer selection against specific antigens [32]. Metal-coated magnetic nanoparticles have been demonstrated to be useful for measurements such as SERS [33, 34]. They have also been utilized for amplification of signal for SPR-based refractive index measurements [35].

Integration of ferromagnetic metal layers with plasmonic substrates can allow more precise control over on-chip capture of these magnetic particles and their subsequent application towards plasmonic or non-plasmonic sensing. Specially for nanostructures, the shape of the structures can have profound effect on the

electromagnetic field [36, 37]. Electrostatic fields exhibit singular behavior near sharp tips due to the lightning rod effect [38]. Electromagnetic fields can also be highly localized near sharp tips made of noble metals by nanofocusing of surface plasmons [39, 40]. Similarly concentration of magnetic fields near sharp tips, leading to singular behavior can be theoretically predicted [41]. Intense highly localized magnetic field and field gradients are very useful for directed capture and concentration of molecules and cells on chip [42–44]. Fabrication of ultrasharp ferromagnetic tips with noble metals such gold and silver can be used to combine their plasmonic and magnetic advantages.

A facile way of fabricating ferromagnetic plasmonic substrates over large regions reproducibly is template stripping [30, 45, 46]. This technique relies on the poor adhesion between noble metals (Au, Ag) and silicon surface. The inverse stencil of desired structures is fabricated on to silicon wafers using standard silicon processing techniques. A noble metal layer is first deposited on the wafer followed by a layer of Nickel. The nanostructures can then be peeled off the silicon mold using an adhesive layer (thermal or UV-curable epoxy) on a substrate of choice. Figure 9 shows wedges and pyramids fabricated on planar glass slides using this method. These structures had a tip with very sharp radius of curvature, close to 10 nm.

Analytical equations derived for these structures demonstrate that the magnetic field close to the tips diverge if the tip radius is close to zero. Computer simulations further show the increase in magnetic field and field gradient close to the tips for

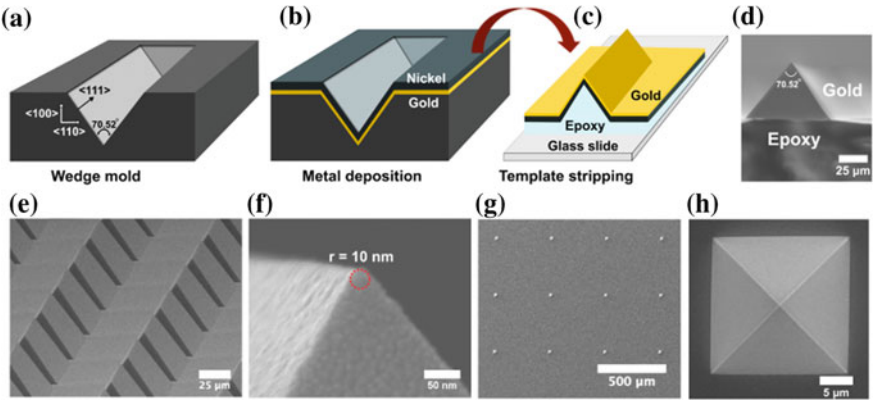

Fig. 9 **a** Wedge-shaped trenches in a silicon mold formed using anisotropic etching of <100> silicon wafer in KOH. **b** Deposition of thin layer of gold followed by thin layer of nickel. **c** UV-curable epoxy was added to the template and a glass slide was placed on top. The sample was then placed under ultraviolet light for curing. The metal film attached to epoxy and glass slide was template-stripped. SEM images showing **d** cross-sectional view of a template-stripped wedge. **e** Bird's eye view of arrays of wedges. **f** Side-view of the tip of a wedge with 10 nm radius of curvature. This wedge had 50 nm gold deposited on top of 125 nm nickel film. **g** Widely separated array of pyramids fabricated using a pyramidal silicon template. **h** Top-down view of a template-stripped pyramid. Adapted from [30]

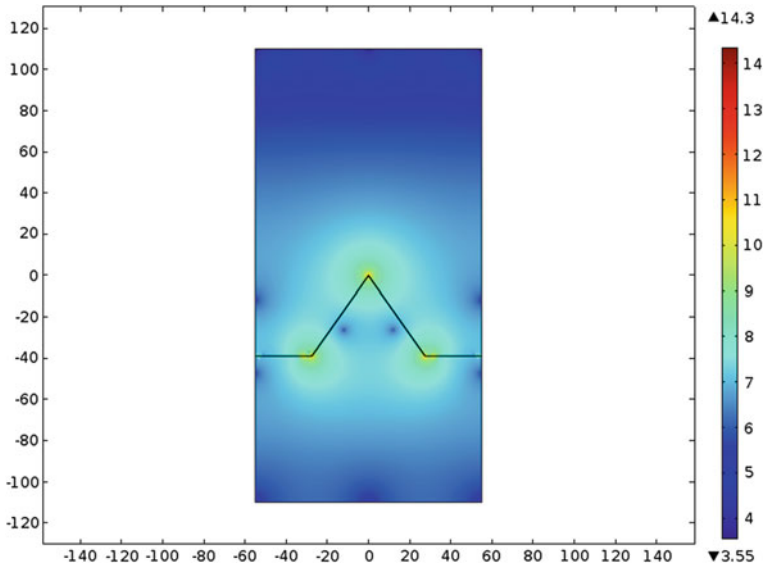

Fig. 10 COMSOL simulation showing order of magnitude plot of gradient of magnetic field (∇H) for a wedge with 10 nm tip radius showing the entire modeled area. Adapted from [30]

various tip radii of curvature. [27, 30] Magnetic particles of various sizes (1.6 μm, 300, and 20 nm) suspended in an aqueous environment were loaded on these substrates and an external magnetic field was introduced. The force experienced by a magnetic particle under the influence of an external magnetic field is directly proportional to the gradient of field. The strong magnetic field close to the sharp tips combined with strong spatial gradient resulted in generation of extremely strong magnetic field gradients near them, directed the particles to be trapped there (Figs. 10, 11). Similar results were obtained for the pyramids. Trapping of single nanoparticles at the pyramidal tips was observed in several cases (Fig. 11d) (Fig. 12).

In order to reveal the plasmonic contribution from the substrates, magnetic nanoparticles labeled with 4-MP were trapped on these substrates. Raman signal was obtained from these molecules and compared with control samples which should not have any contribution towards the enhancement of Raman signal from the molecules. Increased SERS signal from the molecules was observed on the noble metal-coated wedges and pyramids. Hence, these substrates were able to show directed capture of magnetic nanoparticles in a fluidic environment over large areas as well as applications towards plasmonic biosensing. This method can be used for rapid capture of analyte molecules in solution, tagged to magnetic

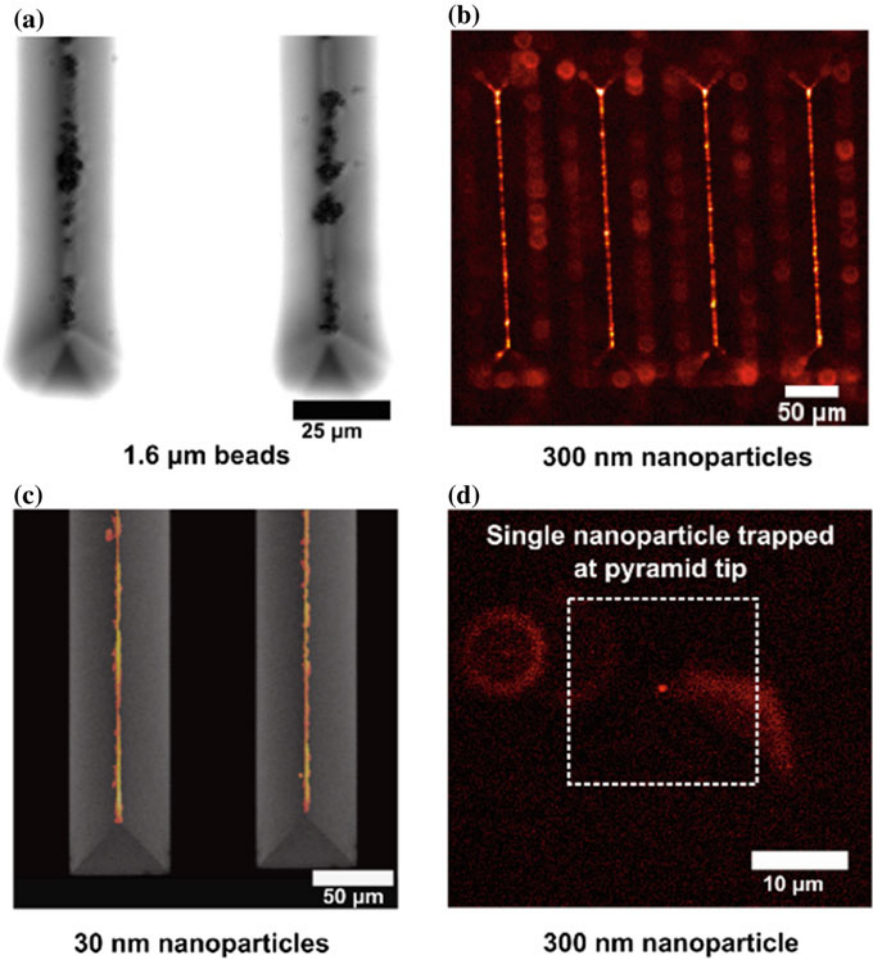

Fig. 11 Images showing the capture of magnetic beads and nanoparticles of various sizes at the tips of magnetic nanostructures. Adapted from [30]

nanoparticles. The molecules are delivered close to the sharp metallic tips, which also serve as plasmonic hotspots. Sharp noble metal tips have been widely used for measurement of tip-enhanced Raman signal [47]. In this case, a high-density of these tips is distributed throughout the substrate and target molecules can be delivered directly to them.

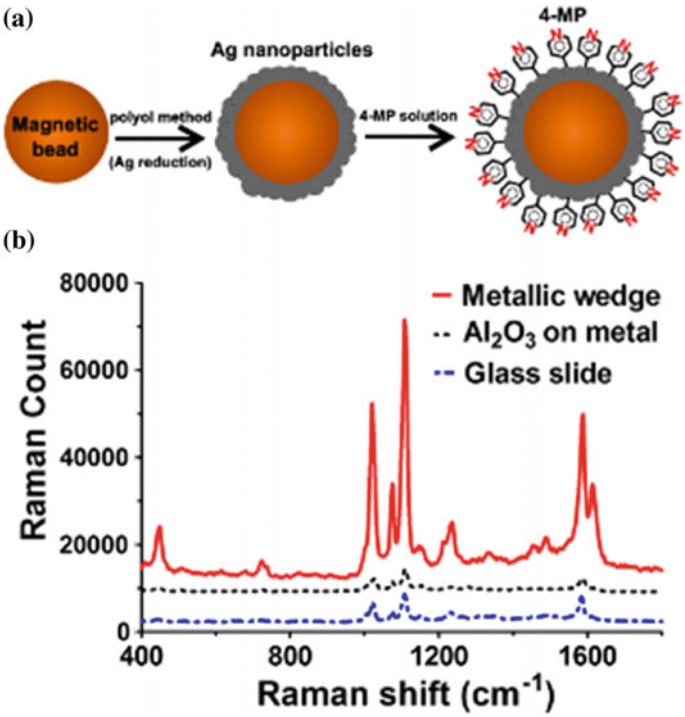

Fig. 12 **a** Cross-sectional schematic showing the chemical functionalization of magnetic beads with 4-mercaptopyrdine (4-MP) after coating them with Ag nanoparticles. **b** Raman signal obtained from the beads captured on SERS-active metallic wedges as compared to on metallic wedges coated with 10 nm of Al_2O_3 and standard glass slide. Glass slides as well as Al_2O_3 coated wedges should not have any contribution towards the SERS signal obtained from the molecules. Adapted from [30]

5 Conclusion

In summary, nanostructured plasmonic substrates which can direct the flow of molecules in solution towards sensing sites can result in drastic improvements in device performance. The limit of detection as well as time taken for sensing can be significantly improved. Three mechanisms for analyte concentration and biosensing were discussed in this chapter. These were based on evaporation, surface-tension and magnetic forces. Localized concentration of molecules near the plasmonic sensing sites was reported for all the cases. Among these techniques, evaporation-dependent directed flow is the simplest as it does not have any preset requirements for surface functionalization of receptors on the sensor surface and does not require integration with external elements such as magnetic beads. It is likely also the slowest among the three concentration mechanisms. Magnetic particle based analyte capture can be extremely fast and has other unique advantages,

such as analyte capture independent of the direction of fluid flow. None of these methods needed external power sources, bulky apparatus, or assemblies. No heating artifacts or solution conductance limitations were encountered, which is often the case with electric field-driven concentration methods.

These methods can be easily used in combination with standard microfluidics or just by addition of a droplet on the chip-surface. Droplet-based methods are advantageous as they are simple to use and have zero dead-volume lacking any fluidic interconnects and hence do not waste a lot of analytes. These substrates can also be used for electrochemical biosensing using the metal layers as electrodes. Furthermore, they have shown potential towards trapping of biological particles such as organelles on chip and studying their properties. Moving further these techniques can lead to the development of point-of-care or commercial nanostructured sensing devices with significantly better performance and improved usability as compared to current state of the art.

References

1. Sheehan PE, Whitman LJ (2005) Detection limits for nanoscale biosensors. Nano Lett 5(4): 803–807
2. Squires TM, Messinger RJ, Manalis SR (2008) Making it stick: convection, reaction and diffusion in surface-based biosensors. Nat Biotechnol 26(4):417–426
3. Escobedo C, Brolo AG, Gordon R, Sinton D (2010) Flow-through vs flow-over: analysis of transport and binding in nanohole array plasmonic biosensors. Anal Chem 82(24): 10015–10020
4. Eftekhari F, Escobedo C, Ferreira J, Duan X, Girotto EM, Brolo AG, Gordon R, Sinton D (2009) Nanoholes as nanochannels: flow-through plasmonic sensing. Anal Chem 81(11): 4308–4311
5. Yanik AA, Huang M, Artar A, Chang T-Y, Altug H (2010) Integrated nanoplasmonic-nanofluidic biosensors with targeted delivery of analytes. Appl Phys Lett 96(2):021101
6. Escobedo C, Brolo AG, Gordon R, Sinton D (2012) Optofluidic concentration: plasmonic nanostructure as concentrator and sensor. Nano Lett 12(3):1592–1596
7. Barik A, Chen X, Oh S-H (2016) Ultralow-power electronic trapping of nanoparticles with sub-10 nm gold nanogap electrodes. Nano Lett 16(10):6317–6324
8. Barik A, Otto LM, Yoo D, Jose J, Johnson TW, Oh S-H (2014) Dielectrophoresis-enhanced plasmonic sensing with gold nanohole arrays. Nano Lett 14(4):2006–2012
9. Deegan RD, Bakajin O, Dupont TF, Huber G, Nagel SR, Witten TA (1997) Capillary flow as the cause of ring stains from dried liquid drops. Nature 389(6653):827–829
10. Ebbesen TW, Lezec HJ, Ghaemi HF, Thio T, Wolff PA (1998) Extraordinary optical transmission through sub-wavelength hole arrays. Nature 391(6668):667–669
11. Barnes WL, Murray WA, Dintinger J, Devaux E, Ebbesen TW (2004) Surface plasmon polaritons and their role in the enhanced transmission of light through periodic arrays of subwavelength holes in a metal film. Phys Rev Lett 92(10)
12. Gao HW, Henzie J, Odom TW (2006) Direct evidence for surface plasmon-mediated enhanced light transmission through metallic nanohole arrays. Nano Lett 6(9):2104–2108
13. Homola J, Yee SS, Gauglitz G (1999) Surface plasmon resonance sensors: review. Sensors Actuators B Chem 54(1–2):3–15
14. Brolo AG, Arctander E, Gordon R, Leathem B, Kavanagh KL (2004) Nanohole-enhanced Raman scattering. Nano Lett 4(10):2015–2018

15. Lesuffleur A, Im H, Lindquist N, Oh S (2007) Periodic nanohole arrays with shape-enhanced plasmon resonance as real-time biosensors. Appl Phys Lett 90(24): 243110
16. Im H, Lee SH, Wittenberg NJ, Johnson TW, Lindquist NC, Nagpal P, Norris DJ, Oh S-H (2011) Template-stripped smooth Ag nanohole arrays with silica shells for surface plasmon resonance biosensing. ACS Nano 5(8):6244–6253
17. Yu QM, Guan P, Qin D, Golden G, Wallace PM (2008) Inverted size-dependence of surface-enhanced Raman scattering on gold nanohole and nanodisk arrays. Nano Lett 8(7): 1923–1928
18. Lee S, Bantz K, Lindquist N, Oh S, Haynes C (2009) Self-assembled plasmonic nanohole arrays. Langmuir 25(23):13685–13693
19. Brolo AG, Kwok SC, Moffitt MG, Gordon R, Riordon J, Kavanagh KL (2005) Enhanced fluorescence from arrays of nanoholes in a gold film. J Am Chem Soc 127(42):14936–14941
20. Saboktakin M, Ye X, Chettiar U, Engheta N, Murray C, Kagan C (2013) Plasmonic enhancement of nanophosphor upconversion luminescence in Au nanohole arrays. ACS Nano 7(8):7186–7192
21. Kumar S, Wittenberg NJ, Oh S-H (2013) Nanopore-induced spontaneous concentration for optofluidic sensing and particle assembly. Anal Chem 85(2):971–977
22. Kumar S, Wolken GG, Wittenberg NJ, Arriaga EA, Oh S-H (2015) Nanohole array-directed trapping of mammalian mitochondria enabling single organelle analysis. Anal Chem 87(24): 11973–11977
23. Handique K, Gogoi BP, Burke DT, Mastrangelo CH, Burns MA (1997) Microfluidic flow control using selective hydrophobic patterning. In: Micromachining and microfabrication. International Society for Optics and Photonics pp 185–195
24. Zhao B, Moore JS, Beebe DJ (2001) Surface-directed liquid flow inside microchannels. Science 291(5506):1023–1026
25. Chitnis G, Ding Z, Chang C-L, Savran CA, Ziaie B (2011) Laser-treated hydrophobic paper: an inexpensive microfluidic platform. Lab Chip 11(6):1161–1165
26. Kumar S, Cherukulappurath S, Johnson TW, Oh S-H (2014) Millimeter-sized suspended plasmonic nanohole arrays for surface-tension-driven flow-through SERS. Chem Mater 26(22):6523–6530
27. Kumar S (2015) Directed transport-enabled improved biosensing and bioanalysis on plasmonic nanostructured substrates. University of Minnesota
28. De Angelis F, Gentile F, Mecarini F, Das G, Moretti M, Candeloro P, Coluccio M, Cojoc G, Accardo A, Liberale C (2011) Breaking the diffusion limit with super-hydrophobic delivery of molecules to plasmonic nanofocusing SERS structures. Nat Photonics 5(11):682–687
29. Yang S, Dai X, Stogin BB, Wong T-S (2016) Ultrasensitive surface-enhanced Raman scattering detection in common fluids. Proc Natl Acad Sci 113(2):268–273
30. Kumar S, Johnson TW, Wood CK, Qu T, Wittenberg NJ, Otto LM, Shaver J, Long NJ, Victora RH, Edel JB, Oh S-H (2016) Template-stripped multifunctional wedge and pyramid arrays for magnetic nanofocusing and optical sensing. ACS Appl Mater Interfaces 8(14): 9319–9326
31. Grancharov S, Zeng H, Sun S, Wang S, O'Brien S, Murray C, Kirtley J, Held G (2005) Bio-functionalization of monodisperse magnetic nanoparticles and their use as biomolecular labels in a magnetic tunnel junction based sensor. J Phys Chem B 109(26):13030–13035
32. Lou X, Qian J, Xiao Y, Viel L, Gerdon AE, Lagally ET, Atzberger P, Tarasow TM, Heeger AJ, Soh HT (2009) Micromagnetic selection of aptamers in microfluidic channels. Proc Natl Acad Sci USA 106(9):2989–2994
33. Jun BH, Noh MS, Kim J, Kim G, Kang H, Kim MS, Seo YT, Baek J, Kim JH, Park J (2010) Multifunctional silver-embedded magnetic nanoparticles as SERS nanoprobes and their applications. Small 6(1):119–125
34. Jun BH, Noh MS, Kim G, Kang H, Kim JH, Chung WJ, Kim MS, Kim YK, Cho MH, Jeong DH, Lee YS (2009) Protein separation and identification using magnetic beads encoded with surface-enhanced Raman spectroscopy. Anal Biochem 391(1):24–30

35. Soelberg SD, Stevens RC, Limaye AP, Furlong CE (2009) Surface plasmon resonance detection using antibody-linked magnetic nanoparticles for analyte capture, purification, concentration, and signal amplification. Anal Chem 81(6):2357–2363
36. Maier SA (2007) Plasmonics: fundamentals and applications. Springer
37. Halas NJ, Lal S, Chang WS, Link S, Nordlander P (2011) Plasmons in strongly coupled metallic nanostructures. Chem Rev 111(6):3913–3961
38. Jackson JD (1998) Classical electrodynamics, 3rd edn. Wiley
39. Stockman M (2004) Nanofocusing of optical energy in tapered plasmonic waveguides. Phys Rev Lett 93(13):137404
40. Gramotnev D, Bozhevolnyi S (2010) Plasmonics beyond the diffraction limit. Nat Photonics 4:83–91
41. Van Bladel J (1983) Field singularities at the tip of a cone. Proc IEEE 71(7):901–902
42. Tanase M, Felton EJ, Gray DS, Hultgren A, Chen CS, Reich DH (2005) Assembly of multicellular constructs and microarrays of cells using magnetic nanowires. Lab Chip 5(6): 598–605
43. Pamme N, Wilhelm C (2006) Continuous sorting of magnetic cells via on-chip free-flow magnetophoresis. Lab Chip 6(8):974–980
44. Chen G, Alberts C, Rodriguez W, Toner M (2010) Concentration and purification of human immunodeficiency virus type 1 virions by microfluidic separation of superparamagnetic nanoparticles. Anal Chem 82(2):723–728
45. Nagpal P, Lindquist NC, Oh S-H, Norris DJ (2009) Ultrasmooth patterned metals for plasmonics and metamaterials. Science 325(5940):594–597
46. Park JH, Nagpal P, McPeak KM, Lindquist NC, Oh S-H, Norris DJ (2013) Fabrication of smooth patterned structures of refractory metals, semiconductors, and oxides via template stripping. ACS Appl Mater Interfaces 5(19):9701–9708
47. Pettinger B (2006) Tip-enhanced Raman spectroscopy (TERS). Surf Enhanc Raman Scatt Phys Appl 103:217–240